Available online at www.sciencedirect.com
ScienceDirect
Optics Communications 270 (2007) 31–40
OPTICS COMMUNICATIONS
www.elsevier.com/locate/optcom

A novel wavelength dispersive device with a dispersive element based on staircase-like straight and parallel arrayed waveguides

Oscar Martínez Matos [a,*], María L. Calvo [a], Pavel Cheben [b,1], Siegfried Janz [b,1], José A. Rodrigo [a], Dan-Xia Xu [b,1], André Delâge [b,1]

[a] Departamento de Óptica, Facultad de Ciencias Físicas, Universidad Complutense de Madrid, 28040 Madrid, Spain
[b] Institute for Microstructural Sciences, National Research Council of Canada, Ottawa, Canada K1A 0R6

Received 29 April 2005; received in revised form 21 August 2006; accepted 24 August 2006

Abstract

We propose a new type of arrayed waveguide grating (AWG) multiplexer/demultiplexer based on modified group refractive index. This device is composed by an array of straight and parallel waveguides of equal length and each waveguide consist of two sections with different width. The length of the two sections are changed from a waveguide to the adjacent one following a linear dependence resulting in a wavelength dispersive waveguide array. An example of the device design for silicon-on-insulator (SOI) platform is provided and numerical simulations have been carried out for various arrayed waveguide parameters. We demonstrate that the group index modification can be used for tailoring device dispersion properties, and that it can also result in new dispersion characteristics predicted numerically not observed in conventional AWGs. Additional advantages are that the demultiplexer does not necessarily require bending waveguide sections as in a conventional AWG (de)multiplexers, and thus yields highly compact devices with potentially very low insertion loss. Channel spacing of 1 nm have been predicted for sub-micron waveguides sizes. In this paper it is also proposed a novel wavefront converter based on waveguide array lens-like element with waveguides broadened sections. Numerical results for different input/output geometries are analized.

Keywords: Optical waveguides; Silicon-on-insulator technology; Wavelength division multiplexing

1. Introduction

The continuous demand for internet and telecommunication services is expected to keep driving the development of wavelength division multiplexed (WDM) networks [1,2]. Wavelength multiplexers and demultiplexers, capable of combining and separating different spectral channels, are the key components of WDM network. Over the last decades the use of the wavelength division multiplexing in optical networks was mostly performed by discrete devices such as thin-film interference filters. The state of the art planar waveguide based mux/demux devices include arrayed waveguide gratings (AWG) [3] and echelle grating devices [4]. These devices are based on waveguides with low refractive index contrast, typically of the order of 1%, between the waveguide core and the cladding, such as those fabricated in silica-on-silicon platform. However, state of the art silica-on-silicon AWGs become prohibitively large for devices with higher channel counts and narrower channel spacing [5], and the integration of different functions on a single chip is not feasible for practical systems, unless the size of the individual functional elements is significantly reduced. Silicon-based photonic waveguide circuits have recently emerged as commercially viable optoelectronics devices [6–8]. In silicon-on-insulator (SOI) waveguide devices, several orders of magnitude reduction of device size can be achieved [9] as compared to devices based on

* Corresponding author. Tel.: +34 91 3944678; fax: +34 91 3944683.
E-mail addresses: omartine@fis.ucm.es, ommatos@fis.ucm.es (O. Martínez Matos), pavel.cheben@nrc-cnrc.gc.ca (P. Cheben).
[1] Tel.: +1 613 9931624; fax: +1 613 9907656.

0030-4018/$ - see front matter
doi:10.1016/j.optcom.2006.08.035

silica-on-silicon materials. This remarkable size reduction is possible because of a very high difference in refractive index between the waveguide core (Si, $n \sim 3.5$) and the surrounding cladding material (typically SiO_2, $n \sim 1.5$). This results in a large index contrast, two orders of magnitude higher than that of standard silica-on-silicon waveguides. This in turn allows to guide light in waveguides with bend radii of the order of several micrometers, or to reduce the waveguide transverse dimensions to or below micrometer range. Various AWG demultiplexers in SOI platform have been demonstrated [6,8–19].

Sub-micron waveguides (also called *photonics wires*) in SOI are feasible technologically and the fabrication methods yield acceptable scattering loss. In the last years, the scattering loss due to sidewall roughness it has been reduced by several methods [12]. Thermal oxidation after reactive ion etching, reduce the residual rms roughness to ~2 nm and yield a loss reduction from 32 dB/cm to 0.8 dB/cm for a 0.5 μm wide SOI waveguide [20]. A deep UV lithography and dry etching the top silicon layer yield losses as low as 2.4 dB/cm for 0.5×0.33 μm^2 waveguides [21]. The advance of nanofabrication technologies is expected to rapidly improve the sub-micron waveguides loss in SOI.

The applicability of photonics wires in optical devices has been demonstrated by several companies (IBM, MIT, OITDA) and research groups. Thermo-optic switches [22], ring resonators [21] and conventional AWG demultiplexers [16] with waveguides wide of 300-nm square cross-section, 500-nm square cross-section and 320-nm thickness with 450-nm width, respectively, have been demonstrated successfully.

Since conventional AWG demultiplexers require curved waveguides, the minimum available bend radius, which in turn is determined by the index contrast, sets the lower limit for the device dimensions. Here we suggest that highly compact demultiplexers are feasible in AWGs comprising an array of parallel straight waveguides. Recently, Kawakita et al. [23] proposed a straight waveguide AWG in which the refractive index is constant for each individual waveguide while it linearly increases from the first to the last waveguide in the phase array. The latter is achieved by the selected area growth of the waveguide layers, resulting in a changing waveguide thickness across the phase array. Fabrication challenges of such approach are obvious.

In this paper we propose a novel mux/demux device with a dispersive element comprising an array of staircase-like straight and parallel sub-micron waveguides in SOI platform, developing further the concept proposed in [19,24]. The wavefront converting properties of the device are also examined. The paper is organized as follows: Section 2 is dedicated to the dispersive element. Wavelength dispersive properties, particularly dependence of the angular dispersion on device geometrical factors and properties of the waveguides are studied, and free spectral range and channel spacing are also discussed. In this section it is also studied the wavelength dispersive properties of an element composed by photonic bandgap waveguide sections of different lengths. Section 3 is dedicated to the geometry of the device. Parameters such as required waveguide lengths and corresponding phase differences are calculated. Discussions and conclusions are presented in Section 4.

2. Dispersive element

The operational principle of the proposed device is analogous to that of a conventional AWG. An incoming beam from the input waveguide is coupled through a slab waveguide combiner into the waveguide array and propagates through each individual waveguide towards the output aperture. An appropriate arrangement of waveguides at the input of the array assures that the in-plane diverging wave in the input slab waveguide is coupled into the arrayed waveguides with equal phase across the entire input aperture of the AWG. In other words, the arc contouring the input of the phase array is geometrically made to coincide with the equiphasal surface of the diverging wavefront.

Fig. 1a shows a general schematics of a demultiplexing device. A dispersive element is located in a waveguide array comprising N waveguides. The geometry shown in Fig. 1a provides for both wavefront converting and wavelength dispersive properties. The former is achieved by transforming a divergent wavefront into a convergent wavefront, so that a real image of the input waveguide aperture front is formed in the focal region of the output combiner slab waveguide. The wavefront transforming element is discussed in Section 3.

The dispersive element provides the wavelength dispersive property required for the separation resp. combination (demultiplexing resp. multiplexing) of different spectral channels. Here the dispersive element is placed in the central (straight waveguide) section of the device (see Fig. 1a and b), and it is composed by an array of parallel straight waveguides of varying width, unlike in conventional AWG devices that demand curved sections in the waveguide array.

We propose a dispersive element where each jth waveguide is divided into three different sections. The first section has a waveguide width W_0 and length L_j; the second section is a waveguide taper of length l', and the third section has a modified waveguide width W_1 and length L'_j. In our design, the respective width of the Sections I and III are kept constant, while the respective lengths of these two sections change linearly between the adjacent waveguides. We define the length increment ΔL ($\Delta L'$) of Section I (Section III) between adjacent waveguides j and $j-1$ as: $\Delta L = L_j - L_{j-1}$ ($\Delta L' = L'_j - L'_{j-1}$). ΔL is constant for all the waveguides, and $\Delta L' = -\Delta L$, so that the total length l of the dispersive element is maintained constant. Taper Section II can be made identical for all waveguides, so that it does not affect demultiplexer dispersion.

To characterize the performance of the dispersive element we first discuss the propagation of an electromagnetic

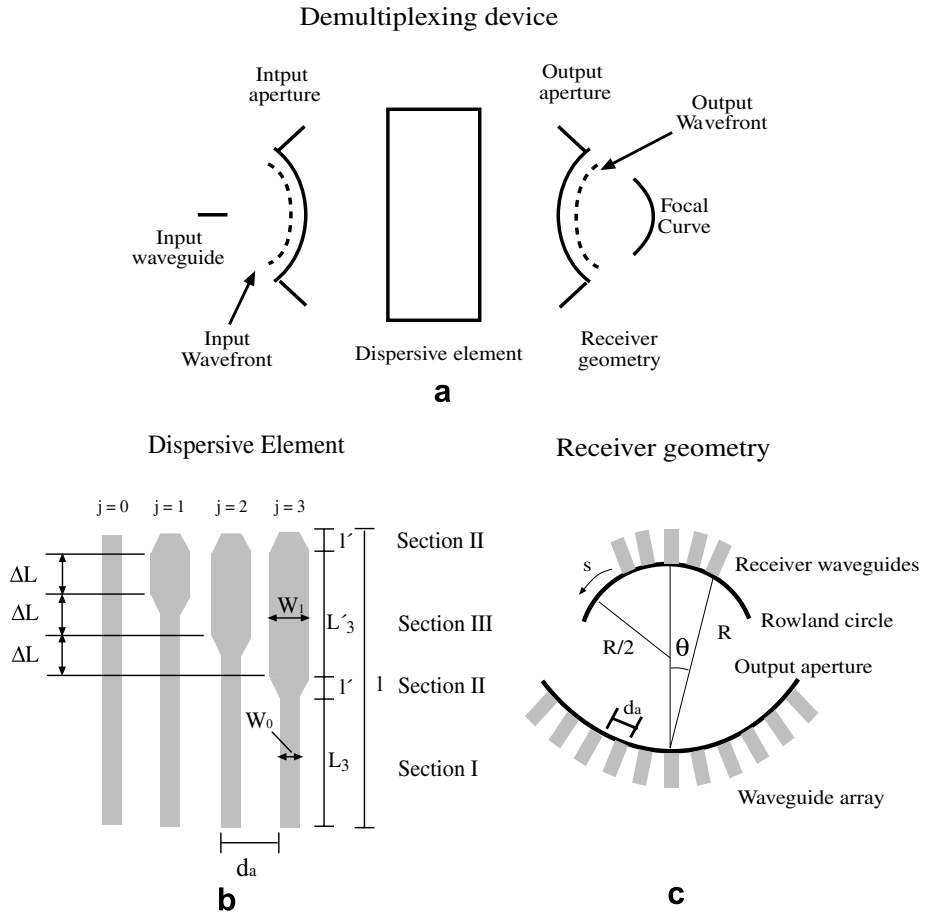

Fig. 1. (a) A general schematics of a demultiplexing device. (b) A schematics showing four adjacent waveguides of the dispersive element. (c) Receiver geometry.

field in each individual etched rib SOI waveguide [25]. Exact values of the mode propagation constants were calculated by a mode solver for different waveguides width. The following waveguide parameters have been used for the simulation: waveguide thickness = 1 μm and ridge etch depth = 0.8 μm. However, for waveguide width less than ~0.5 μm, the etch depth was increased to 1 μm yielding a square waveguide. We assume that waveguides operate in single mode condition. This condition can be reached in high index contrast ridge waveguides by adjusting waveguide cross-section geometry [26] or by proper mode filtering [10,27,28]. Also, adiabatic gradual tapering between the waveguide sections of different width assures that no higher order modes are excited where the two waveguides joint. Under these assumptions it is reasonable to expect that most of the electromagnetic energy propagating along the waveguides is contained in the fundamental waveguide mode and that the device can be modelled by taking into account only the fundamental mode dispersion. The adiabatic tapering also minimizes the insertion loss of the device. SOI tapers with negligible loss and modal conversion using two-step ridge to rectangular tapering have recently been experimentally reported [29], demonstrating that for taper length >50 μm, both the loss penalty (<1%) and the mode conversion are negligible. Similar tapers can be used to minimize the insertion loss due to mode mismatch at the interface between the ridge waveguides and the slab waveguide combiner. Analogous assumptions were made in the analysis of the device geometry in Section 3.

The length difference $\Delta L'$ of the arrayed waveguides is chosen such that the phase difference between adjacent waveguides equals an integer multiple of 2π for the central wavelength λ_c of the demultiplexer. For this λ_c, the signals in the individual waveguides will reach the output aperture with equal phase modulo 2π. The outputs of the arrayed waveguides are located on a circle of radius R, (see Fig. 1c). The dispersion of the demultiplexer is due to the linearly decreasing (increasing) lengths $L_j(L'_j)$ of Sections I and III. The wavelength dependent phase shift between adjacent waveguides produces a wavelength dependent tilt angle of the wavefront in the output combiner, so that different wavelengths converges towards different points along an arc (Rowland circle) of a radius $R/2$ [30].

We denote the effective index in waveguide Sections I and III as $n(\lambda, W)$, with W either W_0 or W_1. The phase shift $\Delta\phi$ between two adjacent waveguides is

$$\Delta\phi(\lambda, W_0, W_1) = 2\pi\lambda^{-1}\Delta L'(n(\lambda, W_1) - n(\lambda, W_0)). \quad (1)$$

By requiring that the phase shift between the adjacent waveguides is constant for all the waveguides and equals an integer multiple of 2π for the central wavelength λ_c we obtain

$$\Delta L'(\lambda_c, m, W_0, W_1) = \lambda_c m/(n(\lambda_c, W_1) - n(\lambda_c, W_0)), \quad (2)$$

where m is the order of the phase array.

Using (1)–(2) with angle dispersion relation (see e.g. Smit and Van Dam [3]) and the approximation $\sin(x) \sim x$, it is obtained for the wavefront tilt angle θ

$$\theta(m, \lambda, W_0, W_1) = M(m, \lambda_c, W_0, W_1)(n_{FPR} d_a)^{-1} \Delta\lambda, \quad (3)$$

where n_{FPR} is the effective mode index in the free propagating slab waveguide region and d_a is the waveguide pitch where the array joins the output combiner (see Fig. 1c). Here we have considered only the Taylor expansion to the first order in $\Delta\lambda = \lambda - \lambda_c$. M in (3) is the modified grating order defined by

$$M(\lambda_c, m, W_0, W_1) = m \frac{\widetilde{N}_g(\lambda_c, W_1) - \widetilde{N}_g(\lambda_c, W_0)}{n(\lambda_c, W_1) - n(\lambda_c, W_0)}, \quad (4)$$

and $\widetilde{N}_g(\lambda, W)$ is the group index:

$$\widetilde{N}_g(\lambda, W) = n(\lambda, W) - \lambda \frac{dn(\lambda, W)}{d\lambda}. \quad (5)$$

The modified interference order M as defined in (4) has a significance analogous to a modified grating in a conventional arrayed waveguide grating [3] and it governs the device wavelength dispersion characteristics. However, in addition to the parameters determining dispersion in a conventional AWG such as (m, n_{FPR}, d_a), here dispersive properties allow for an additional degree of freedom provided by the group index and effective index differences in the numerator and denominator of (4), respectively.

Demultiplexing characteristics of the proposed device will now be examined for a dispersive element designed for the SOI platform ($n_{core} = 3.476$, $n_{cladding} = 1.5$, at 1550 nm) and with $d_a = 3$ μm and $n_{FPR} = 3.44$. The experimental parameters considered here, including number of waveguides, waveguide width and gaps, have been used in some of the AWG devices previously fabricated in SOI platform [9]. The effective mode indices in the SOI waveguides have been calculated numerically by a mode solver.

Fig. 2 shows the waveguide width dependences of the *group index* and the *effective index*. We observe a monotonic growing dependence of the *effective index* that approaches an asymptotic value for bulk silicon for large waveguide width. The *group index* reaches a maximum value for waveguides width = 0.3 μm and with increasing W asymptotically approaching the *effective index* curve. It is interesting to note that when waveguide dimensions are reduced, the modes became delocalized. This effect has important implications on waveguide geometry design.

From (4) and Fig. 2 it is obvious that (de)multiplexer dispersion can be controlled by adjusting the *group index* and the *effective index* values for different sections (I and III, in Fig. 1b), for example by a proper selection of the

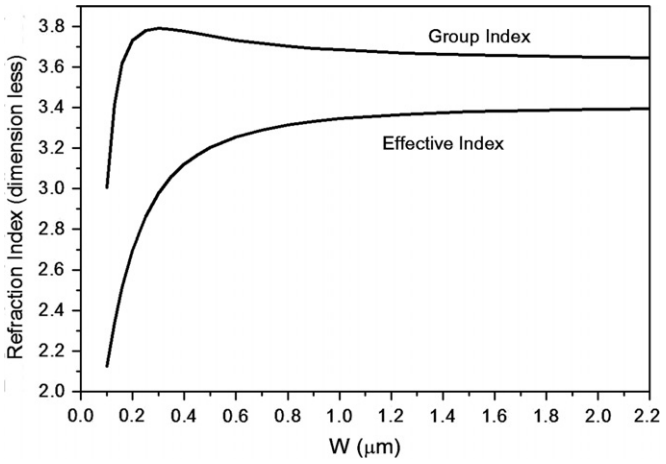

Fig. 2. Group index and effective index dependences in SOI waveguides of different width for $\lambda_c = 1550$ nm.

width W_0 and W_1 of the staircase-like waveguides of the AWG. It is interesting to notice that one can advantageously use other waveguide modification that would result in an alteration of group and/or effective indices. We will discuss this below.

Fig. 3 shows dependence of the modified order number M (for $m = 1$) on the width of the waveguide broadened section W_1 for different sub-micron width $W_0 = 0.1$ μm, 0.3 μm, 0.5 μm and 0.8 μm. Indeed, width $W_0 = 0.1$ μm is not feasible for practical mux/demux devices because the waveguide mode becomes delocalized as the waveguide cross-section shrinks. But here we include waveguide width $W_0 = 0.1$ μm to discus below the anomalous dispersion behaviour. We observe that dispersion increases for small values of the width W_0 and W_1 if $M > 0$, and for large values W_0 and W_1 if $M < 0$. $M > 1$ can also be reached as in a conventional AWG. In this paper we analyze an example of a demultiplexer with straight waveguides. However, the dispersion enhancement effect due to group index modification can be applied to enhance dispersion of a conventional AWG.

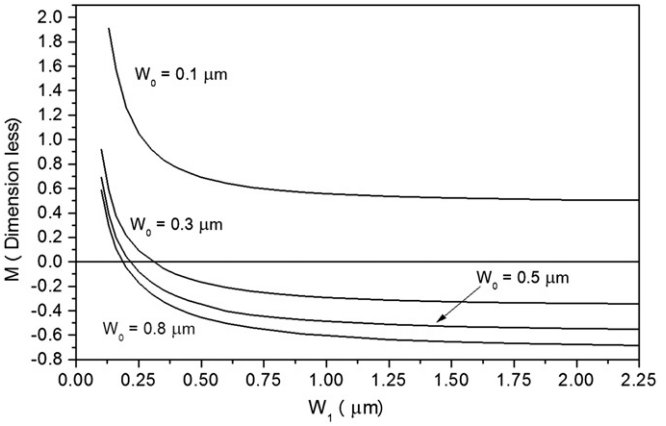

Fig. 3. Modified order M as a function of waveguide width W_1 for different width W_0. $W_0 = 0.1$, 0.3, 0.5, 0.8 μm.

Positive and negative values of M are obtained depending on W_0 and W_1. This sign change would make a change on dispersion properties with respect to the device optical axis ($\theta = 0$) yielding an inverted spectrum. The spectrum inversion effect is unique for this type of wavelength dispersive device.

Fig. 4 shows spectral dependence of dispersion angle θ. Parameters values (indicated on the figure caption) have been chosen in such a way that condition (2) is satisfied for a length difference $\Delta L' = 100$ μm keeping the size of the dispersive element constant. It also has been considered $|M| = 3.8$ yielding a constant channel spacing of ~2.45 nm. Dispersion angle dependence is linear for all curves as expected for a Taylor expansion to first order in $\Delta\lambda$. Spectrum inversion (negative curve slope) can be seen in curve a for demultiplexer device with $W_0 = 0.1$ μm, $W_1 = 0.103$ μm, and $m = 2$.

By proper selection on W_0 and W_1 we can design the free spectral range (FSR) $\Delta\lambda_{\mathrm{FSR}} = (\lambda_{m-1}, \lambda_{m+1})$ for which the demultiplexing device changes the interference order m to $m-1(\lambda_{m-1})$ or to $m+1(\lambda_{m+1})$. Vertical lines in Fig. 4 indicate the calculated values (λ_{m-1}, λ_{m+1}). In our analysis $\Delta\lambda_{\mathrm{FSR}}$ is inversely proportional to M. It is interesting to notice anomalous dispersion behaviour of this device. It is a known property of a diffraction grating or an AWG that free spectral range FSR $= \lambda_c/m$, so that large interference orders, though beneficial for high spectral resolution, reduce the FSR. Here it is shown that in a demultiplexer based on waveguide broadening there is an anomalous dependence of FSR on interference order m. By comparing curves a and b corresponding to devices with orders $m = 2$, 19, 8, 5, it is obvious that the FSR does not follow λ_c/m dependence and it is actually similar for the three devices.

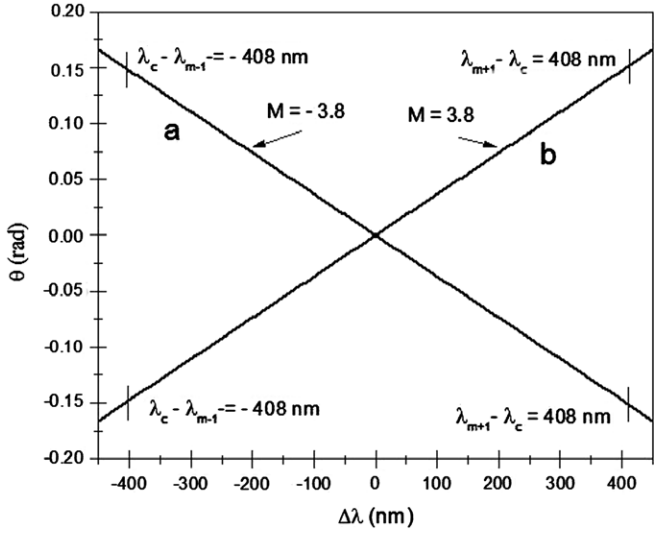

Fig. 4. Dispersion angle θ for four different dispersive element geometries as a function of $\Delta\lambda$, where $\lambda_c = 1550$ nm. The four devices are designed to have $|M| = 3.8$ and $\Delta L' = 100$ μm. Curve a correspond to $W_0 = 0.1$ μm, $W_1 = 0.103$ μm, $m = 2$, and curve b correspond to three different devices: ($W_0 = 0.3$ μm, $W_1 = 0.588$ μm, $m = 19$), ($W_0 = 0.5$ μm, $W_1 = 0.855$ μm, $m = 8$) and ($W_0 = 0.8$ μm, $W_1 = 2.251$ μm, $m = 5$). The wavelengths corresponding to the FSR are indicated by the short vertical lines.

In a particular case of $M \sim 0$ (i.e. $\widetilde{N}_g(\lambda_c, W_1) \sim \widetilde{N}_g(\lambda_c, W_0)$), the device is non-dispersive to the first order in $\Delta\lambda$. This situation applies even for $m \neq 0$, in which case it would be required to use instead of approximated Eq. (3) a rigorous formula. Preliminary results indicates that dispersion angle dependence for $M \sim 0$ will not be linear obtaining a curve that contains parts with positive and negative slopes, yielding identical dispersion angles value for wavelengths on different sides of the zero slope angle. This interesting property can be used to combine two channels in the same receiver waveguide. Moreover, the nonlinear behaviour on dispersion angle can be relevant for increasing FSR and the channels count. This anomalous FSR is a unique property of this kind of device based on waveguide broadening.

In the following we will estimate the channel spacing for different mux/demux geometries. As it is observed from Eqs. (2) and (4), device dimension and dispersive properties scales inversely with $n(\lambda_c, W_1) - n(\lambda_c, W_0)$ and hence an optimum combination (M, $\Delta L'$) or equivalently of (W_0, W_1, m, $\Delta L'$) needs to be found to achieve the conditions of high dispersion and small size. We estimate the minimum channel spacing (CS) as

$$\mathrm{CS}(\lambda_c, m, W_0, W_1) = 1.22\lambda_c/(NM(\lambda_c, m, W_0, W)), \tag{6}$$

where we have used a simple Rayleigh criterion, according to which the half-width x of the diffraction pattern is [31]

$$x = 1.22\lambda R(Dn_{\mathrm{FPR}})^{-1}, \tag{7}$$

where $D = Nd_a$ is the output aperture of the AWG, N is the number of the arrayed waveguides with a pitch d_a and R is the focal distance (see Fig. 1c).

We consider the SOI waveguide parameters as defined and $N = 201$, $R = 1$ mm, $d_a = 3$ μm and $D = 600$ μm. Fig. 5 shows the AWG channel spacing as a function of W_1.

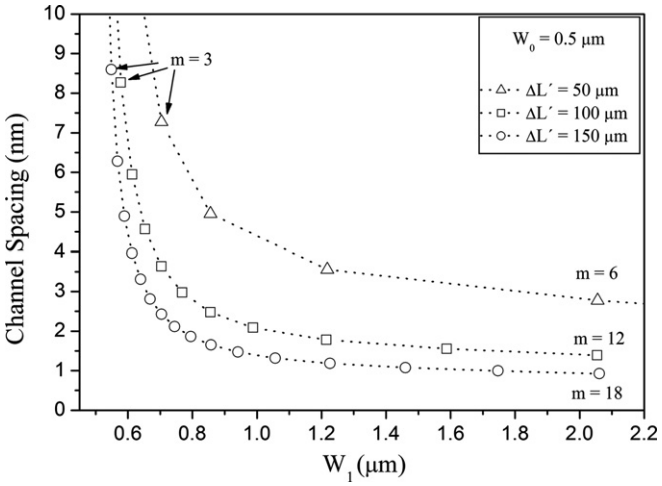

Fig. 5. Channel spacing versus waveguide width W_1. Length values $\Delta L'$ are shown in the inset of the figure. All data points are calculated for a width $W_0 = 0.5$ μm and m values associated to each data are shown in the figure.

Triangle square and circle data points correspond to $\Delta L' = 50$, 100 and 150 μm, respectively. The data have been calculated for a waveguide width $W_0 = 0.5$ μm. The points shown in Fig. 5 satisfy condition (2) for all m. This condition is useful for exploring demultiplexing capability of the device keeping its size constant. For a given $\Delta L'$, m increases with the modified waveguide width W_1, as does the channel count. Channel spacing converges to an asymptotic value as m increases. For $\Delta L' = 150$ μm, the asymptotic value is nearly reached for $m = 14$, yielding the channel spacing of 1 nm (circle data points). As expected, channel spacing decreases with increasing length difference $\Delta L'$. For example, for $W_1 \sim 1.2$ μm the channel spacing changes from 3.56 nm to 1.22 nm when $\Delta L'$ increases from 50 to 150 μm. Nevertheless, by keeping W_0 and W_1 constant the channel number follows the m^{-1} behaviour as in conventional AWG.

Channel spacing dependence on W_1 is shown in Fig. 6 for different values of W_0. Circle, square, up triangle and down triangle data points show the obtained values for $W_0 = 0.1$, 0.3, 0.5 and 0.8 μm, respectively, for a length difference of $\Delta L' = 100$ μm.

It is observed in Figs. 5 and 6 that for waveguide width of sub-micron sizes (for example: ($N = 201$, $W_0 \sim 0.3$ μm, $W_1 \sim 1.0$ μm, $\Delta L' \sim 100$ μm) or ($N = 201$, $W_0 \sim 0.5$ μm, $W_1 \sim 1.45$ μm, $\Delta L' \sim 150$ μm)), channel spacing of ~1 nm can be achieved. Notice that four different m values (see horizontal line in Fig. 6) produces the same channel spacing ~2.45 nm for the same size of the dispersive element. Those values were used to graph the curves shown on Fig. 4. We can estimate the scattering loss for the dispersive element ($N = 201$; $\Delta L' = 100$ μm; $W_0 = 0.5$ μm; $W_1 = 0.855$ μm; $m = 8$; channel spacing ~2.45 nm (see Fig. 6)) as ~2 dB for a reactive ion etching fabrication method or ~5 dB for a deep UV lithography fabrication method. The introduction of this dispersive element in a conventional AWG will improve dispersion properties [19] yielding a total diffraction loss ~6 dB.

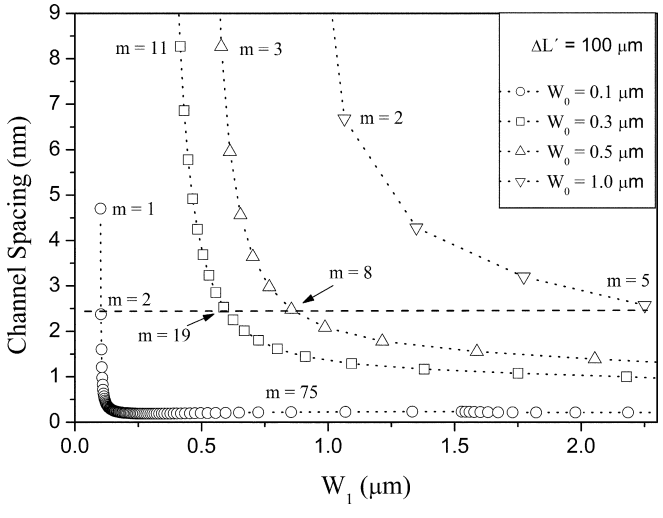

Fig. 6. Channel spacing as a function of width W_1 for different values of the parameter W_0 (see inset). All data points are calculated for $\Delta L' = 100$ μm and m values associated to data points are shown. Horizontal line indicates four devices with the same channel spacing = 2.45. Parameters of these devices are (W_0, W_1, m) = (0.1 μm, 0.103 μm, 2), (0.3 μm, 0.588 μm, 19), (0.5 μm, 0.855 μm, 8) and (0.8 μm, 2.251 μm, 5).

It should be noted that the proposed device is intrinsically polarization dependent. Polarization dependence due to modal birefringence depends on cladding stress (usually SiO_2) and on waveguide geometrical factors. It can be estimated ~0.1 for a 10 nm change in waveguide width for sub-micrometer strip waveguides [32]. Cladding stress is of several hundreds MPa and exerts a force on the Si ridge that modifies the refractive index of the waveguide via the elastooptic effect. Xu et al. demonstrated that the stress-induced birefringence in Si ridge [32,33] (with widths 1.6 and 2.5 μm) and photonic wire waveguides [34] can be used to eliminate the waveguide geometrical birefringence controlling cladding deposition conditions or with thermal anneals [35]. This technique can be used to reduce polarization dependence of the device proposed in this paper for application where polarization insensitivity is demanded.

It is particularly attractive to consider a group index modification by inserting a waveguide section with photonic bandgap waveguides as they can exhibit a very large group index. Not limited to the straight waveguide geometry discussed in this paper, such waveguide sections with large group index can also be placed in the phase array of a conventional AWG, as it is shown in Fig. 7. In what follows, we calculate dispersion enhancement due to the dispersive element with a modified group index given by a photonic bandgap SOI waveguide reported by NTT [36] with $N_g \sim 90$ at 1520 nm, inserted in a 9 channel SOI AWG device.

The main characteristics of the 9 channel SOI AWG device are: the phased array comprises 100 ridge wave-

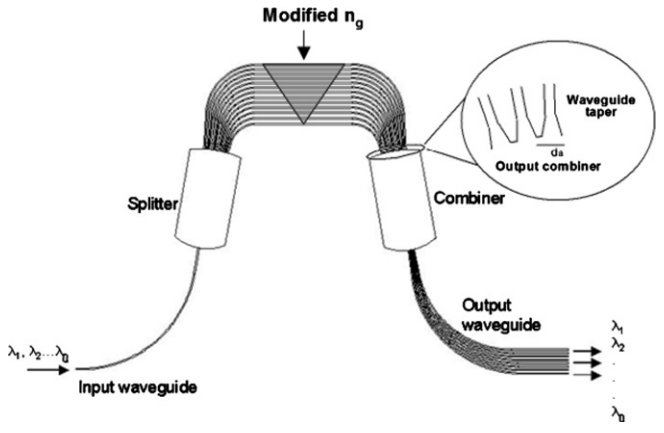

Fig. 7. Dispersion enhancement in a conventional AWG due to the dispersive element with a modified group index given by a photonic bandgap SOI waveguide. The waveguide group index is modified within the indicated triangular-shaped region of the phased array. The inset shows a diagram of the output aperture of the AWG. d_a is the pitch of the array.

guides with a nominal width of 2 μm and with a linear length increment of $\Delta L = 22.68$ μm, a grating order of $m = 49$ and a modified order $M = 50$ hence with a free spectral range of 31 nm. Minimum separation between the arrayed waveguides is 4 μm at both ends of the phased array. The arrayed waveguide are tapered from a nominal width of 2 μm to 3 μm at the ends of the array. The calculated linear dispersion is 0.044 μm/GHz. The separation between the output waveguides at the output coupler focus located at the Rowland circle mount is 8.8 μm and the focal length of the combiner (coupler) slab regions is 1.5 mm. This design gives a Gaussian pass-band with a 200 GHz channel spacing and a calculated crosstalk of <-30 dB, a total diffraction loss of -4 dB, and channel nonuniformity of 0.2 dB. The same design yields an 18 channel device at 100 GHz grid providing the separation between the output waveguides at the Rowland circle is reduced from 8.8 μm to 4.4 μm. Further design details and experimental results have been published elsewhere [37].

Upon inserting our dispersive element given by a photonic bandgap SOI waveguide with a group index of ~90 at 1520 nm [36] into the phased array of the AWG, the modified AWG dispersion is increase according to (3)–(4). Fig. 8 shows dispersion enhancement calculated in the SOI AWG described above for two different length increment ΔL between the photonic bandgap SOI waveguides. A nonlinear dependence of $\widetilde{N}_g(\lambda)$, as in Fig. 4b of Ref. [36], was used for numerical calculations. A large enhancement of AWG angular dispersion is observed in Fig. 8 illustrating the potential of the proposed dispersion mechanism. The future work will address detailed device design and optimization, including detailed simulation of photonic bandgap waveguides and mode matching between the conventional and the photonic bandgap waveguides.

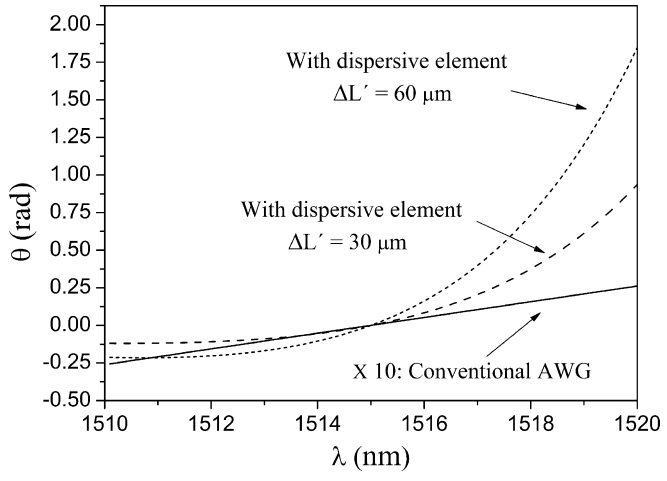

Fig. 8. Dispersion enhancement in an AWG device by waveguide group index modification. Dispersive element with a modified group index by photonic bandgap effect is inserted into the phased array of a conventional AWG as it is schematically shown in Fig. 7. Dispersion enhancement is calculated for the length differences $\Delta L'$ between the adjacent waveguides with modified group index of 30 μm and 60 μm. Data for nonlinear dependence of $\widetilde{N}_g(\lambda)$ was taken from Ref. [36]. For clarity, dispersion of the conventional AWG is showed in the figure increased by a factor 10.

3. Lens-like waveguide wavefront converter

In this section we present a *lens-like* waveguide wavefront converter that provides light focalization in the output combiner slab waveguide by forming a real image of the origin of the divergent wavefront at the focal region of the output combiner. The operational principle of the *lens-like* wavefront converter is based on waveguide broadening sections in the arrayed waveguides (see Fig. 9), similar to that of the dispersive element discussed in previous section. Wavefront converter devices have been studied previously by our research group [38–40].

Each waveguide is composed by two sections of different width, W_0 (the narrower width with a length L_j for the waveguide j) and W_1 (the wider width), both connected by an adiabatically tapered section not shown in the figure. The device operates as a wavefront converter for a specific central wavelength $\lambda_c = 1550$ nm. We assume that the taper structure is the same for all the waveguides of the device, thus introducing a constant phase factor for all the waveguides at a particular wavelength. We do not include this factor in the following analysis as its influence can be simply accounted for and factored out.

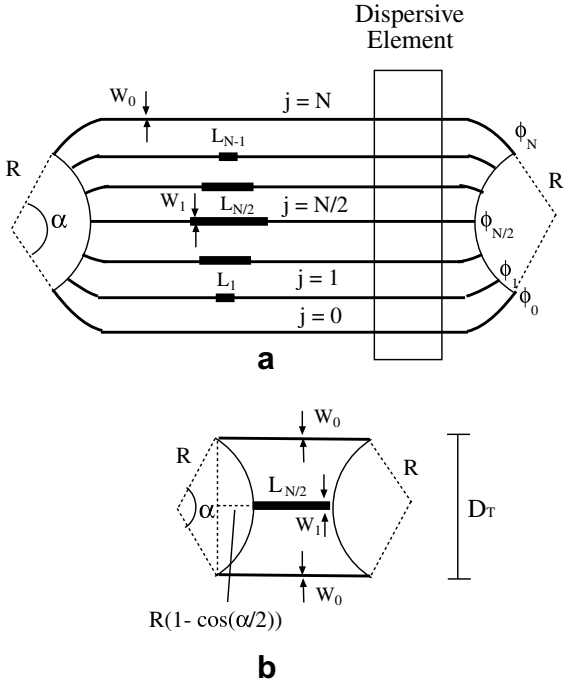

Fig. 9. (a) Representation of a divergent-convergent AWG *lens-like* converter. Input and output focal points are located at the centre of arcs defining the input and output apertures, respectively. Dispersive element can be included at the position shown in the figure, and it is discussed in Section 2. (b) Simplified schematics of the divergent-convergent AWG lens-like wavefront converter, showing only central, $N/2$th, and the marginal waveguides.

Now we introduce convenient lengths of the widened waveguide sections W_1 so that the optical paths through all the waveguides are identical. Hence, the phases of the light emerging at the output aperture of the device (ϕ_j at λ_c for waveguide j) are identical to that along the input array aperture, which in turn guarantees that the light is brought into focus at the output combiner. To simplify the analysis here we omit the bended fan-out and fan-in sections of the input and output of the array, respectively, as it is shown in Fig. 9b. In order to minimize device dimensions, we assume the central waveguide comprising only one section of a widened width W_1.

The modal dispersion will obviously affect the device performance for $\lambda \neq \lambda_c$, and the *lens-like* geometry proposed will be intrinsically dispersive. The phase at different waveguides of the array output aperture will be a function of the position across the array aperture. Unlike in the dispersive element we discussed in Section 2, our aim here is to minimize such chromatic dependences. Analyzing the phase shift between the waveguides at the output aperture, as the wavelength changes, one can quantify the deviation of the device focusing performance from the optimal condition. The largest phase difference at the output aperture will obviously be between the central waveguide $\phi_{N/2}(\lambda)$ and the extreme waveguides ($\phi_N(\lambda)$ or $\phi_0(\lambda)$). We will now quantify these phase differences and will use them to study the focal light distribution.

We first calculate the length $L_{N/2}$ of width W_1, for a device operating as a wavefront converter at central wavelength λ_c. To do this we first demand equal phases for the wavelets at the ends of the central and external waveguides of the array: $\phi_{N/2}(\lambda_c) = \phi_N(\lambda_c)$, with a similar condition imposed for other waveguides:

$$\left[L_{N/2} + 2R\left(1 - \cos\left(\frac{\alpha}{2}\right)\right)\right] n(\lambda_c, W_0) = L_{N/2} n(\lambda_c, W_1). \quad (8)$$

From (8), the length of the central waveguide is obtained as

$$L_{N/2} = 2R\left(1 - \cos\left(\frac{\alpha}{2}\right)\right) \frac{n(\lambda_c, W_0)}{n(\lambda_c, W_1) - n(\lambda_c, W_0)}. \quad (9)$$

According to (9) and considering only the Taylor expansion to the first order in $\Delta\lambda = \lambda - \lambda_c$ the phase shift $\Delta\phi_M(\lambda) = \phi_{N/2}(\lambda) - \phi_N(\lambda)$ is

$$\Delta\phi_M(\lambda, W_0, W_1) = A(\Delta\lambda, W_0, W_1) B(D_T, \alpha), \quad (10)$$

where $A(\Delta\lambda, W_0, W_1)$, is defined as

$$A(\Delta\lambda, W_0, W_1) = \frac{(n(\lambda_c, W_1)\widetilde{N}_g(\lambda_c, W_0) - n(\lambda_c, W_0)\widetilde{N}_g(\lambda_c, W_1))}{n(\lambda_c, W_1) - n(\lambda_c, W_0)} \frac{\Delta\lambda}{(\lambda_c)^2}, \quad (11)$$

accounting for dispersive properties, while $B(D_T, \theta)$, is defined as:

$$B(D_T, \alpha) = 2\pi D_T \tan(\alpha/4), \quad (12)$$

accounting for the input/output geometry (see Fig. 9).

To analyze the dispersion properties of the wavefront converter, we consider the same parameters as in the dispersive element, i.e. $N = 201$, $d_a = 3$ μm, and $D_T = 600$ μm. To assess the performance of the element, we define a figure of merit FM $= AD_T/\Delta\lambda$, as it is observed that for FM $\to 0$ the dispersion effect and device size are minimized while the bandwidth is maximized. Fig. 10 shows the normalized $AD_T/\Delta\lambda$ dependence with waveguide width W_1 for different values of $W_0 = 0.1$, 0.3, 0.5, and 0.8 μm.

FM ~ 0 and hence small dispersion can be obtained when both W_0 and W_1 are reduced, which we attribute to mode delocalization from the core. Examples of the dispersion for various wavefront converting elements are shown in Table 1. We calculate $L_{N/2}$ and $\Delta\phi_M/\Delta\lambda$ using the parameter values W_0 and W_1 used in previous section in Fig. 4 and defined by the horizontal line in Fig. 6. R is calculated using trigonometric relation maintaining $D_T = 600$ μm for different values of α.

The results in Table 1 confirms an intuitively expected fact that minimizing the wavefront curvature at the input of the array (by increasing R that in turn results in a shorter $L_{N/2}$ and a reduced phase shifts $\Delta\phi_M(\lambda)$) a wavefront converter with acceptable achromatic imaging can be obtained. We can choose an approximate criterion for acceptable performance of the wavefront transforming device that the maximum allowed value for $\Delta\phi_M(\lambda)$ produces a focal intensity, that is not less than one half of the intensity value obtained at central wavelength (where $\Delta\phi_M(\lambda_c) = 0$). Hence, by a simple model can be demonstrated that the maximum acceptable phase error is $\Delta\phi_M(\lambda) = 2.8$ rad from which we estimate the maximum allowed range $\Delta\lambda_M$ shown in Table 1. These results confirm that the proposed lens-like wavefront converting elements can be used for geometries with relatively small wavefront curvatures, or for devices operating over a limited wavelength range (bandwidth) when $W_0 > 0.1$ μm. These limitations can be avoided when the waveguide width W_0 and W_1 of the con-

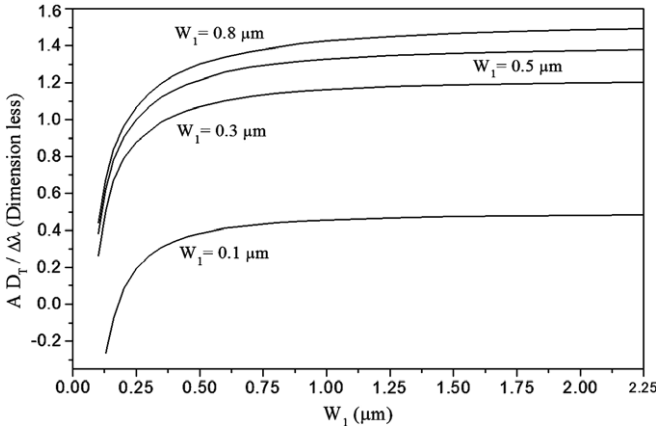

Fig. 10. $AD_T/\Delta\lambda$ dependence with waveguide width W_1 for different values of $W_0 = 0.1$, 0.3, 0.5, 0.8 μm. Notice a large differences between small values W_1 for curves $W_0 = 0.1$ μm and curves with $W_0 > 0.1$ μm. $\Delta\lambda$ is expressed in nm.

Table 1
Dispersion properties for different geometries of lens-like waveguide wavefront converters

		$R = 0.5$ mm	$R = 1.0$ mm	$R = 5.0$ mm
		$\alpha = 1.27$ rad	$\alpha = 0.61$ rad	$\alpha = 0.12$ rad
$W_0 = 0.1$ μm	$\Delta\phi_M/\Delta\lambda$ (rad)	−0.61	−0.28	−0.056
$W_1 = 0.103$ μm	$L_{N/2}$ (mm)	14	6.4	1.2
	$\Delta\lambda_M$ (nm)	4.6	9.8	50.4
$W_0 = 0.3$ μm	$\Delta\phi_M/\Delta\lambda$ (rad)	2.25	1.05	0.21
$W_1 = 0.588$ μm	$L_{N/2}$ (mm)	2.0	0.9	0.2
	$\Delta\lambda_M$ (nm)	1.24	2.6	13.6
$W_0 = 0.5$ μm	$\Delta\phi_M/\Delta\lambda$ (rad)	2.72	1.27	0.25
$W_1 = 0.855$ μm	$L_{N/2}$ (mm)	5.1	2.4	0.5
	$\Delta\lambda_M$ (nm)	1.03	2.2	11.3
$W_0 = 0.8$ μm	$\Delta\phi_M/\Delta\lambda$ (rad)	3.16	1.45	0.29
$W_1 = 2.251$ μm	$L_{N/2}$ (mm)	8.5	3.9	0.8
	$\Delta\lambda_M$ (nm)	0.89	1.9	9.7

verting elements yields $A \sim 0$, but the influence of the mode delocalization effect (growing mode size as the waveguide cross-section shrinks) has to be taken into account. Another possibility we are currently investigating is exploring low dispersion region $M \sim 0$ for $m \neq 0$ as discussed in previous section. Yet another possibility is to use a wavefront converter based on the so-called *zero order* AWG device geometry [41] that is intrinsically non-dispersive, but it demands curved waveguide sections.

4. Conclusions

We have presented a new type of arrayed waveguide grating device comprising a wavelength dispersive element and a wavefront converter. The dispersive element consists of the array of straight and parallel staircase-like waveguides of equal length. The dispersive properties are achieved by splitting the waveguide array into sections with different width, hence obviating the use of curved waveguide sections indispensable in conventional AWG demultiplexers, potentially yielding very compact devices. The waveguide birefringence arising from using different waveguide crosssection can be counterbalanced by cladding stress-induced elasto-optical effect [32]. An example of the device designed for silicon-on-insulator (SOI) platform is provided. We have demonstrated that simple waveguide parameters such as length difference $\Delta L'$, width W_0 and W_1, and resulting effective and group indices, can be used to control demultiplexer properties such as wavelength dispersion, channel spacing and free spectral range (FSR). We have also proposed inserting in the phased array a section with photonic bandgap waveguides exhibiting large group index. Not limited to the straight waveguide geometry discussed in this paper, the waveguide sections with large group index can also be placed in the phase array of a conventional AWG. This significantly enhance dispersion (more than one order of magnitude) and markedly reduced device size, particularly when working in large interference orders required for dense channel spacing.

We also proposed a novel wavefront converter, compatible with the dispersive element, and based on waveguide array *lens-like* element with waveguides broadened sections. We found that because of its intrinsically dispersive properties, the potential use of the *lens-like* geometry element may be restricted for applications with relatively narrow bandwidth.

Acknowledgements

The financial supports from the Spanish Ministry of Science and Technology under Project TIC2002-1846 and from the National Research Council of Canada are acknowledged. Partial results were presented at the V Ibero-American Optics Meeting (RIAO) and VIII OPTILAS, October 2–8, 2004, Porlamar (Venezuela).

References

[1] John Y. Wei, IEEE J. Sel. Areas Commun. 20 (4) (2002) 768.
[2] Jing Zhang, Biswanath Mukherjee, IEEE Network (2004) 41.
[3] M.K. Smith, C. Van Dam, IEEE J. Sel. Top. Quantum Elect. 2 (2) (1996) 236.
[4] S. Janz, A. Balakrishnan, S. Charbonneau, P. Cheben, M. Cloutier, A. Delâge, K. Dossou, L. Erickson, M. Gao, P. Krug, B. Lamontagne, M. Packirisamy, M. Pearson, D.-X. Xu, Technol. Lett. 16 (2004) 503.
[5] S. Janz, M. Pearson, B. Lamontagne, L. Erickson, A. Delâge, P. Cheben, D-X. Xu, M. Gao, A. Balakrishnan, J. Miller, S. Charbonneau, in: OSA Trends in Optics and Photonics, vol. 70, 2002, p. 69 (Optical Fiber Communication Conference, OSA Technical Digest, 2002).
[6] R.R. Whiteman, A.P. Knights, D. George, I.E. Day, A. Vonsovici, A.A. House, G.F. Hopper, M. Asghari, in: Optoelectronic Integration on SiliconProc.SPIE, vol. 4997, 2003, p. 146, Photonocs West, San Jose.
[7] L. Pavesi, D.J. Lockwood, Silicon Photonics, Springer-Verlag, New York, 2004.
[8] G.T. Reed, A.P. Knights, Silicon Photonics – An Introduction, Wiley, 2004.
[9] P. Cheben, D-X Xu, S. Janz, A. Delâge, Proc. SPIE 5117 (2003) 147 (VLSI Circuits and Systems; Jose F. Lopez, Juan A. Montiel-Nelson, Dimitris Pavlidis (Eds.), 2003).

[10] M.R.T. Pearson, A. Bezinger, A. Delâge, J.W. Fraser, S. Janz, P.E. Jessop, D.–X. Xu, SPIE Proc. 3953 (2000) 11.
[11] S. Janz, in: Silicon Photonics, Springer-Verlag, Berlin, 2004 (Chapter 10).
[12] P. Cheben, in: M.L. Calvo, V. Lakshminarayanan (Eds.), Optical Waveguides: From Theory to Applied Technologies, Taylor & Francis Ltd., 2006 (Chapter 5).
[13] P.D. Trinh, S. Yegnanarayanan, F. Coppinger, B. Jalali, IEEE Photon. Technol. Lett. 9 (1997) 940.
[14] P. Cheben, A. Delâge, L. Eirckson, S. Janz, D.-X. Xu, SPIE Proc. 4293 (2001) 15.
[15] P. Cheben, D.-X. Xu, S. Janz, A. Delâge, D. Dalacu, in: D.J. Robbins, G.E. Jabbour (Eds.), Optoelectronic Integration on Silicon, SPIE Proc, vol. 4997, 2003, p. 181.
[16] K. Sasaki, F. Ohno, A. Motegi, T. Baba, Electron. Lett. 41 (2005) 801.
[17] P. Cheben, I. Powell, S. Janz, D.-X. Xu, Opt. Lett. 30 (2005) 1824.
[18] D.-X. Xu, P. Cheben, B. Lamontagne, S. Janz, W.N. Ye, in: 12th International Symposium on SOI Technology and Devices, ECS Proc. 2005-03, 2005, p. 207.
[19] O. Martinez Matos, M.L. Calvo Padilla, P. Cheben, S. Janz, J.A. Rodrigo Martin-Romo, D.-X. Xu, A. Delâge, J. Lightwave Technol. 24 (3) (2006) 1551.
[20] K.K. Lee, D.R. Lim, L.C. Kimerling, J. Shin, F. Cerrina, Opt. Lett. 26 (2001) 1888.
[21] P. Dumon, W. Bogaerts, V. Wiaux, J. Wouters, S. Beckx, J.V. Campenhout, D. Tailaert, B. Luyssaert, P. Bienstman, D.V. Thourhout, R. Baets, IEEE Photon. Lett. 16 (5) (2004) 1328.
[22] T. Chu, H. Yamada, S. Ishida, Y. Arakawa, Opt. Exp. 13 (25) (2005) 10109.
[23] Y. Kawakita, T. Saitoh, S. Shimotaya, K. Shimomura, IEEE Photon. Technol. Lett. 16 (1) (2004) 144.
[24] O. Martinez Matos, M.L. Calvo, P. Cheben, A. Delâge, S. Janz, D.-X. Xu, SPIE Proc. 5622 (2004) 885 [*5th Iberoamerican Meeting on Optics and 8th Latin American Meeting on Optics, Lasers, and Their Applications*, Venezuela, 2004].
[25] W. Snyder, J.D. Love, Optical Waveguide Theory, Chapman and Hall, London, 1983 (Chapter 11).
[26] R.A. Soref, J. Schnidtchen, K. Petermann, IEEE J. Quantum Electron. 27 (1991) 1971.
[27] T. Erdogan, J. Lightwave Technol. 15 (8) (1997) 1277.
[28] C.R. Giles, J. Lightwave Technol. 15 (8) (1997) 1391.
[29] P. Cheben, A. Bogdanov, A. Delâge, S. Janz, B. Lamontagne, M.J. Picard, E. Post, D.-X. Xu, SPIE 5644 (2004) 103.
[30] H.A. Rowland, Phil. Magazine 13 (1882) 469–474. Reprinted in H.A. Rowland, The Physical Papers of Henri August Rowland, The John Hopkins University press, Baltimore, 1902, p. 487.
[31] M. Born, E. Wolf, Principles of Optics, Pergamon press, 1975 (Chapter 7).
[32] D.-X. Xu, P. Cheben, D. Dalacu, A. Delâge, S. Janz, B. Lamontagne, M.J. Picard, W.N. Ye, Opt. Lett. 29 (2004) 2384.
[33] W.N. Ye, D.-X. Xu, S. Janz, P. Cheben, M.-J. Picard, B. Lamontagne, N.G. Tarr, J. Lightwave Technol. 23 (2005) 1308.
[34] D.-X. Xu, J.-M. Baribeau, P. Cheben, D. Dalacu, A. Delâge, B. Lamontagne, S. Janz, M.-J. Picard, W.N. Ye, Electrochem. Soc. Proc. 2004–07 (2004) 619.
[35] D.-X. Xu, S. Janz, P. Cheben, M.-J. Picard, B. Lamontagne, N.G. Tarr, W.N. Ye, in: Proceedings LEOS IEEE Annual Meeting, vol. 2, 2003, p. 590.
[36] M. Notomi, K. Yamada, A. Shinya, J. Takahashi, C. Takahashi, I. Yokohama, Phys. Rev. Lett. 87 (25) (2001) 253902-1.
[37] D.-X. Xu, P. Cheben, D. Dalacu, A. Delâge, S. Janz, B. Lamontagne, M.-J. Picard, W.N. Ye, Opt. Lett. 29 (2004) 2384.
[38] P. Cheben, M.L. Calvo, J. Opt. Soc. Am. 13A (1) (1996) 131.
[39] M.L. Calvo, L. De Pedraza, J. Mod. Opt. (UK) 43 (6) (1996) 1261.
[40] P. Cheben, M.L. Calvo, JOSA A 10 (12) (1993) 2573.
[41] R. Adar, C.H. Henry, C. Dragone, R.C. Kistler, M.A. Mildbrodt, J. Lightwave Technol. 11 (2) (1993) 212.